

Supporting Information

Tetranuclear and dinuclear phenoxido bridged copper complexes based on unsymmetrical thiosemicarbazone ligands

J. A. Isaac, A-T. Mansour, R. David, A. Kochem, C. Philouze, S. Demeshko, F. Meyer, M. Réglie, A. J. Simaan, S. Caldarelli, M. Yemloul, H. Jamet, A. Thibon-Pourret, and C. Belle

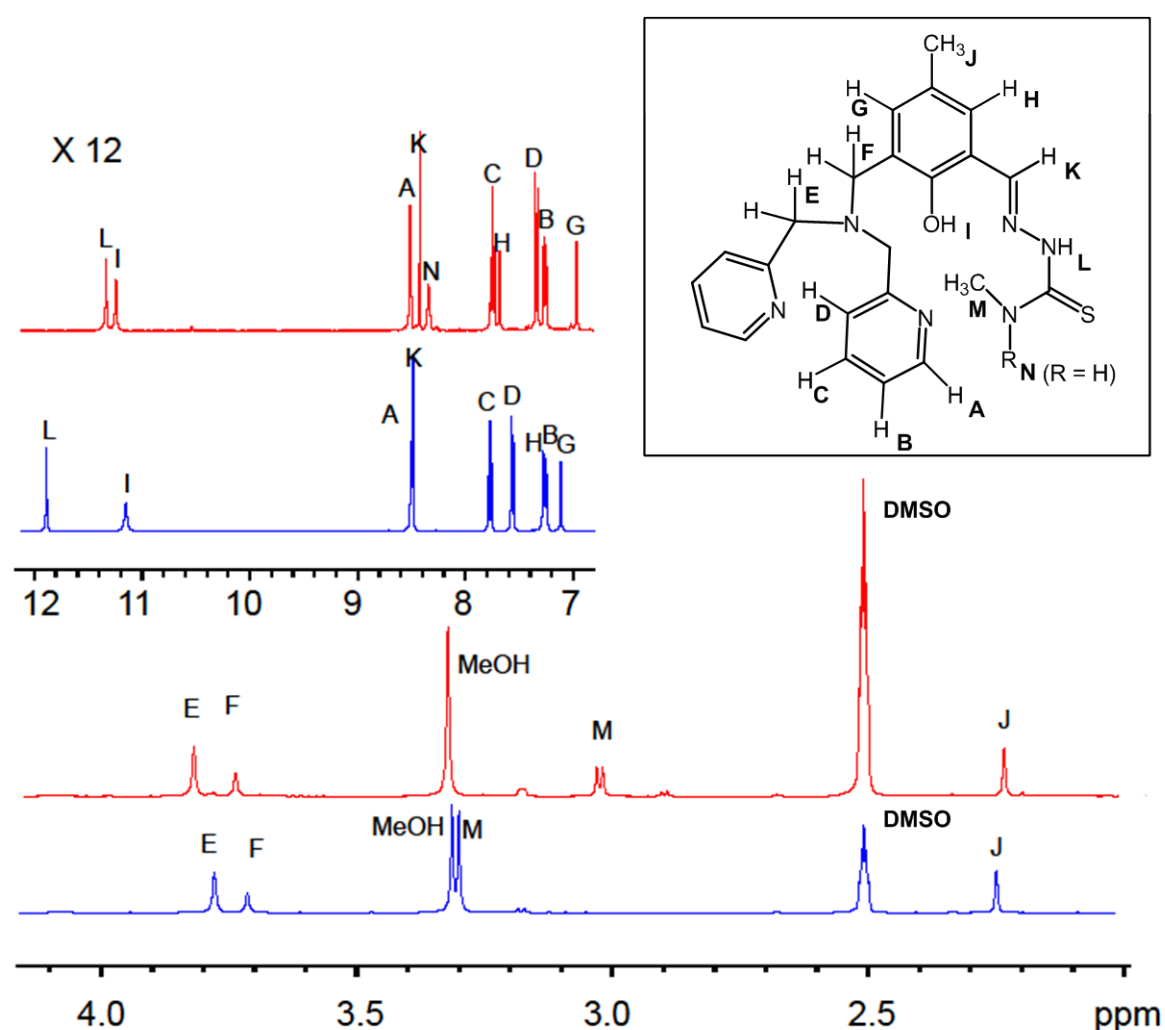


Figure S1. ¹H NMR spectra of ligand L^{MeH} (red) and L^{Me2} (blue) taken in DMSO-*d*₆ at 298 K. Insert: numbering scheme.

Description of the packing for complexes 1t et 2d. Concerning complex **1t**, triflate and acetonitrile molecules are located inside channels which are evidenced when looking at the packing down the b or c axis (Fig. S2A). Each of the tetranuclear Cu(II) complexes are in interaction with two triflate ions via hydrogen bonding starting from the terminal amine group of the thiosemicarbazone arm. Two additional hydrogen bonds link the hydroxido bridges with acetonitrile molecules (Fig S3). There is no clear evidence for interactions between the molecular group constituted with the tetranuclear Cu(II) complex and the four additional molecules.

Intermolecular interactions in the case of complex **2d** are quite simple: there is an hydrogen bond starting from the hydroxido bridge of the dinuclear Cu(II) complex to one oxygen atom of the triflate ion. The triflate ion displays another hydrogen bond with a water molecule (Fig S4). The dinuclear complex molecules interact through double bonds and sulfur atom π stacking which is evidenced when looking at the packing down the c axis (Fig S2B or S5). The distance between the planes of the cycles is about 3.119 Å. The triflate ions and water molecules fill channels located at the corners of the cell while looking down the a axis (Fig S2B).

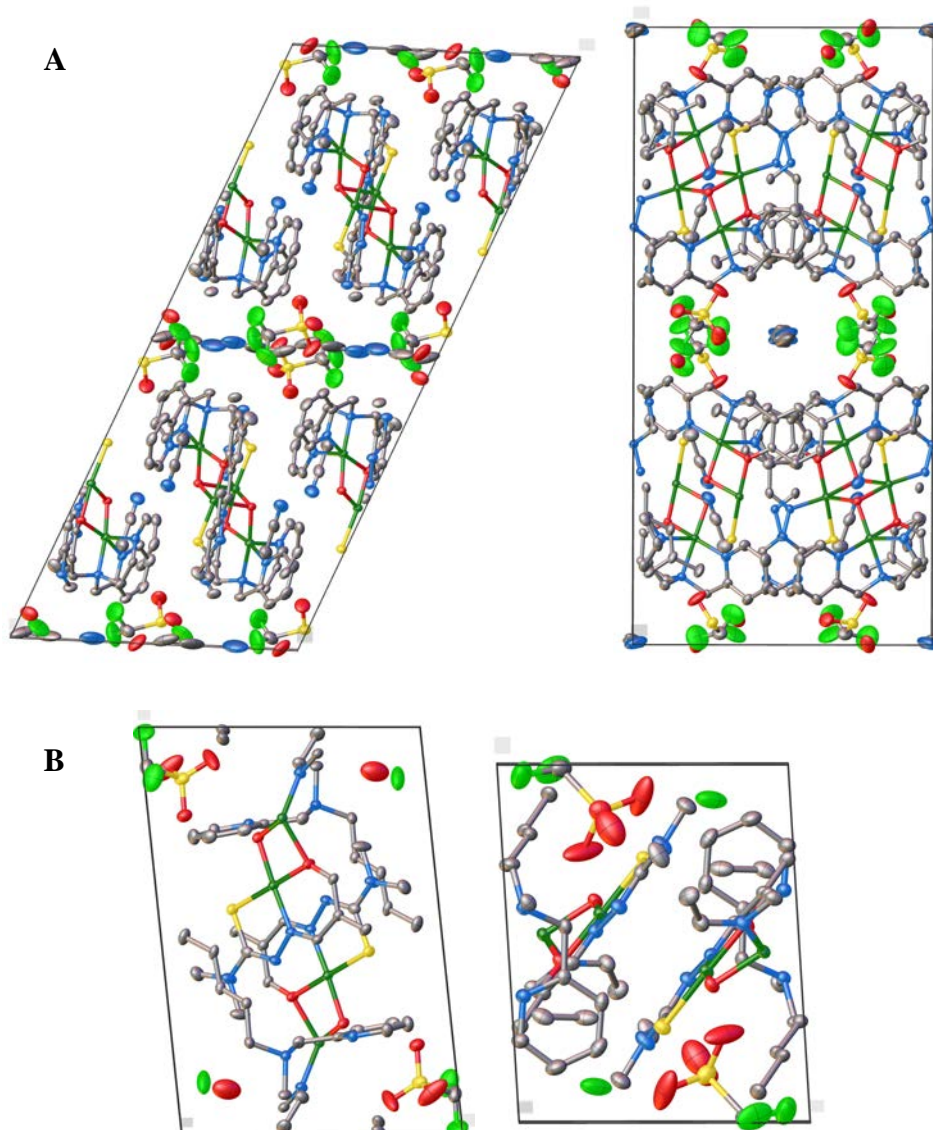


Figure S2. (A): views of the packing of complex **1t** inside the cell, down axis b (left) and c (right); (B) views of the packing of complex **2d** inside the cell, down axis a (left) and c (right).

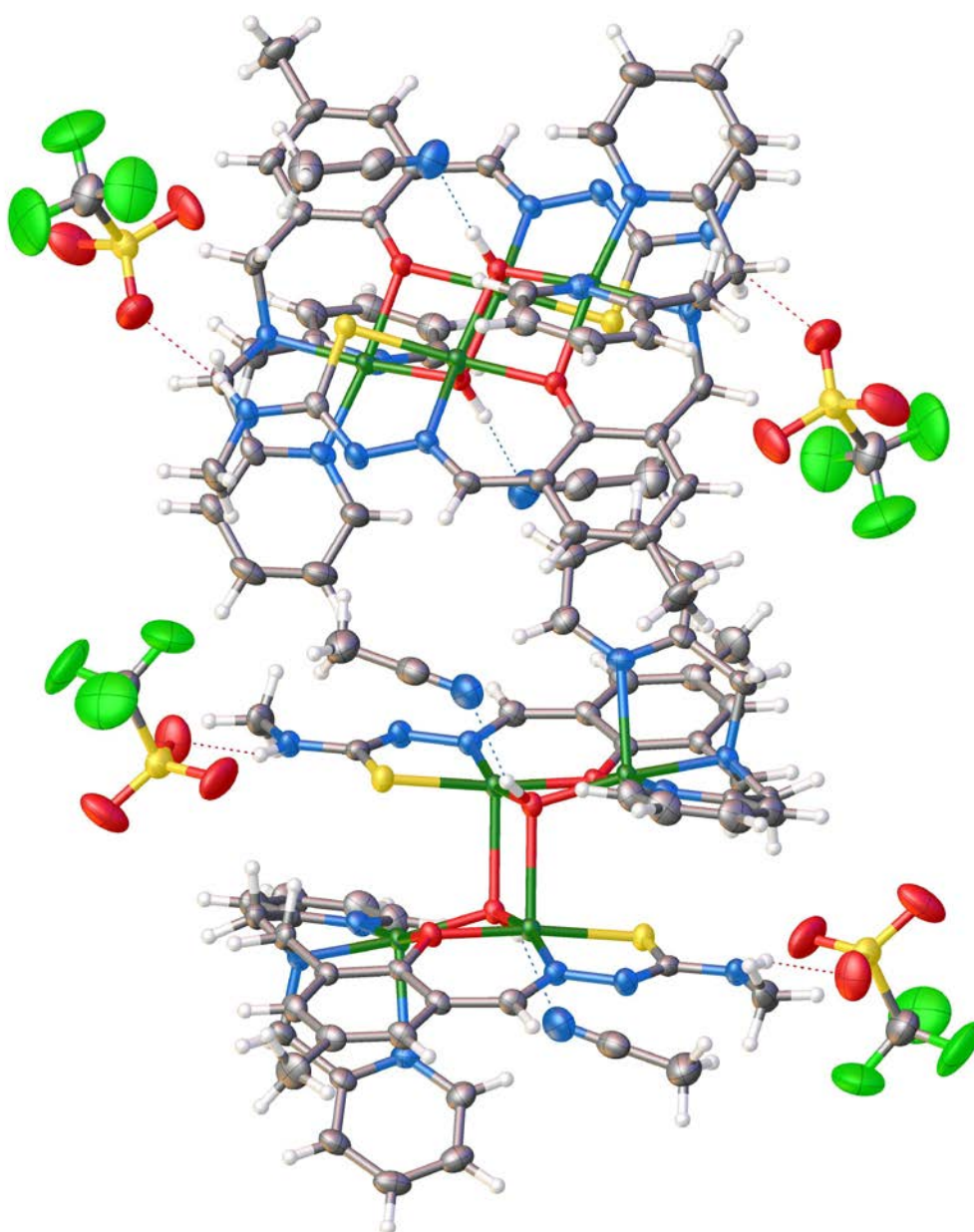


Figure S3. Representation of hydrogen bond network for compound **1t**

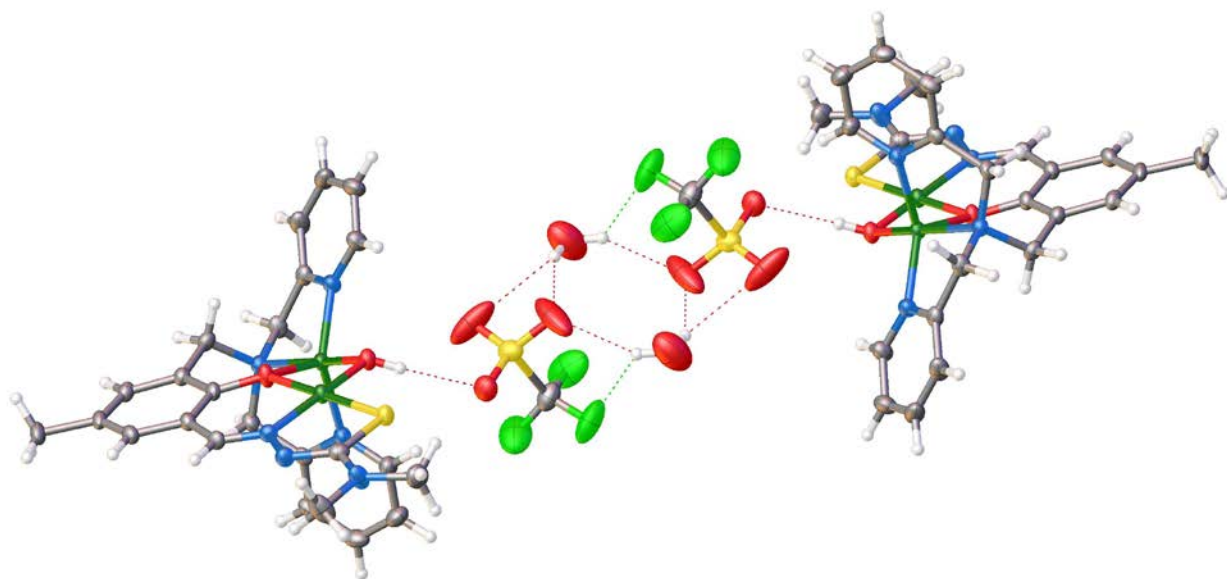


Figure S4. Representation of hydrogen bond network for compound **2d**

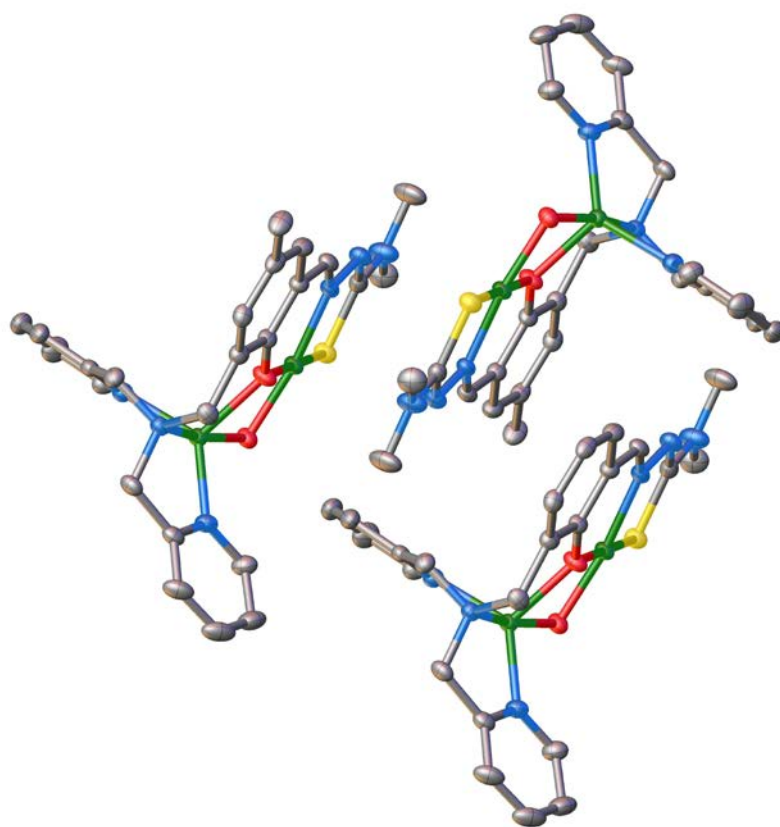


Figure S5. Representation of π stacking for compound **2d** (water and triflate molecules were removed for clarity)

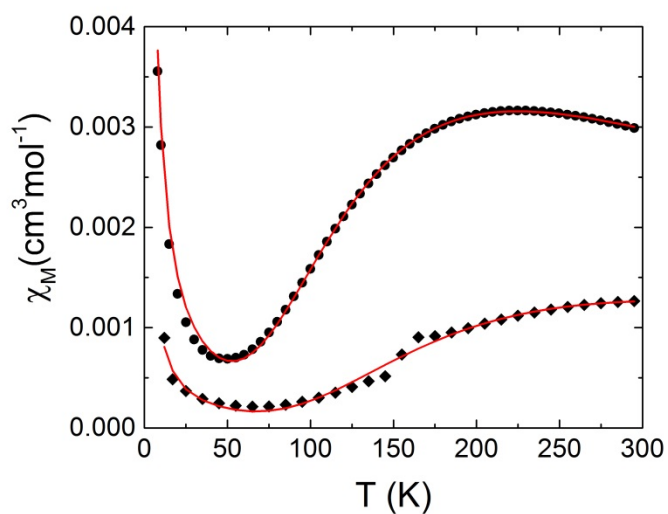


Figure S6. Plots of χ_M vs T for complexes **1t** (black circles) and **2d** (black diamonds). The red solid lines represent the best fits obtained for each sample.

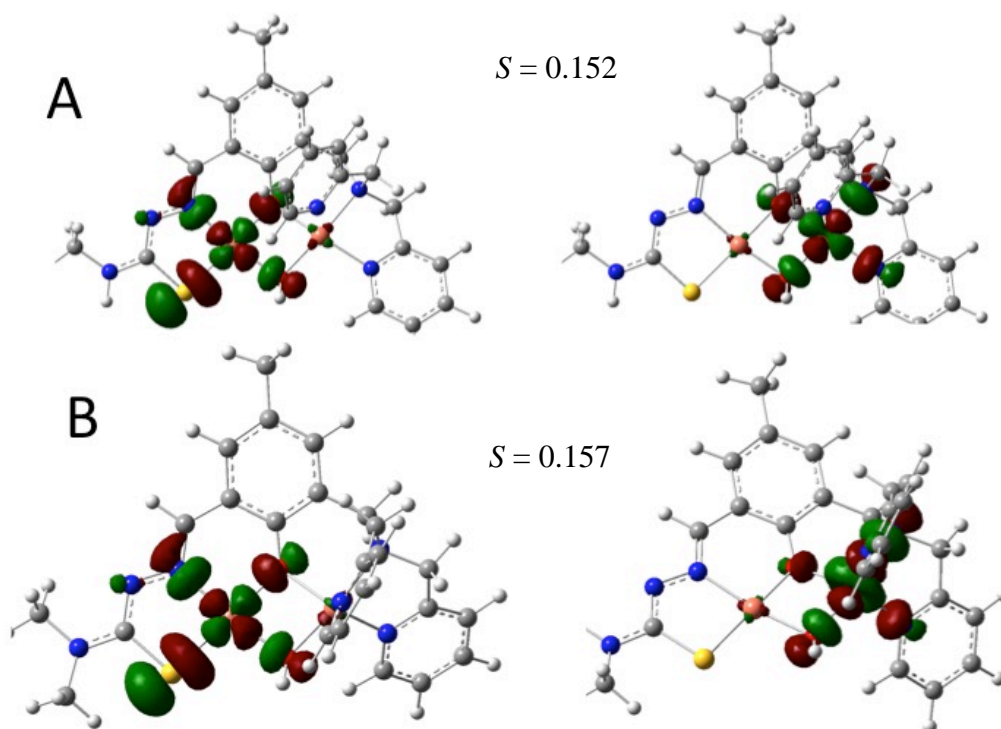


Figure S7. Magnetic orbitals for the broken-symmetry state of (A) **1d** (B) **2d**. Color scheme: Cu orange, S yellow, N dark blue, O red, C dark grey, and H grey. S values represent the spatial overlaps between the magnetic orbitals.

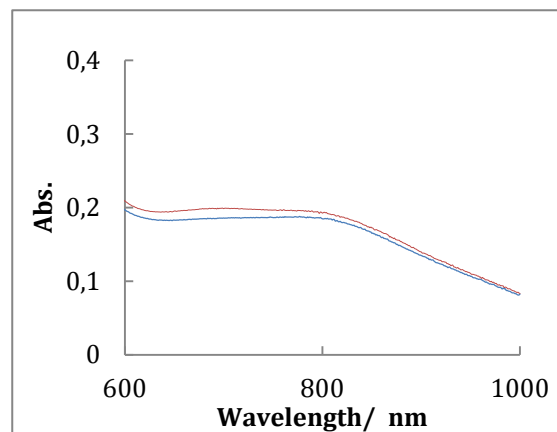
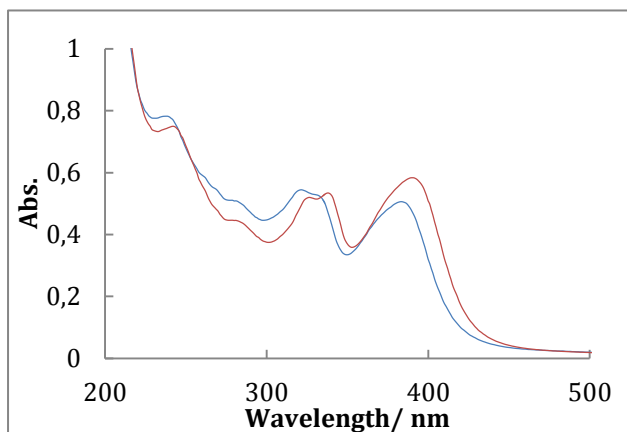


Figure S8. UV-vis spectra in CH₃CN of [Cu₂(L^{MeH})(μ-OH)₂(OTf)₂ (**1t**) in bleu and [Cu₂(L^{Me2})(μ-OH)](OTf) (**2d**) in red. Concentrations : [Cu₂(L^{MeH})(μ-OH)₂(OTf)₂ (**1t**) left : 1.7×10^{-5} mol.dm⁻³, right : 5.3×10^{-4} mol.dm⁻³, [Cu₂(L^{Me2})(μ-OH)](OTf) (**2d**) left : 3.3×10^{-5} mol.dm⁻³, right 1.1×10^{-3} mol.dm⁻³.

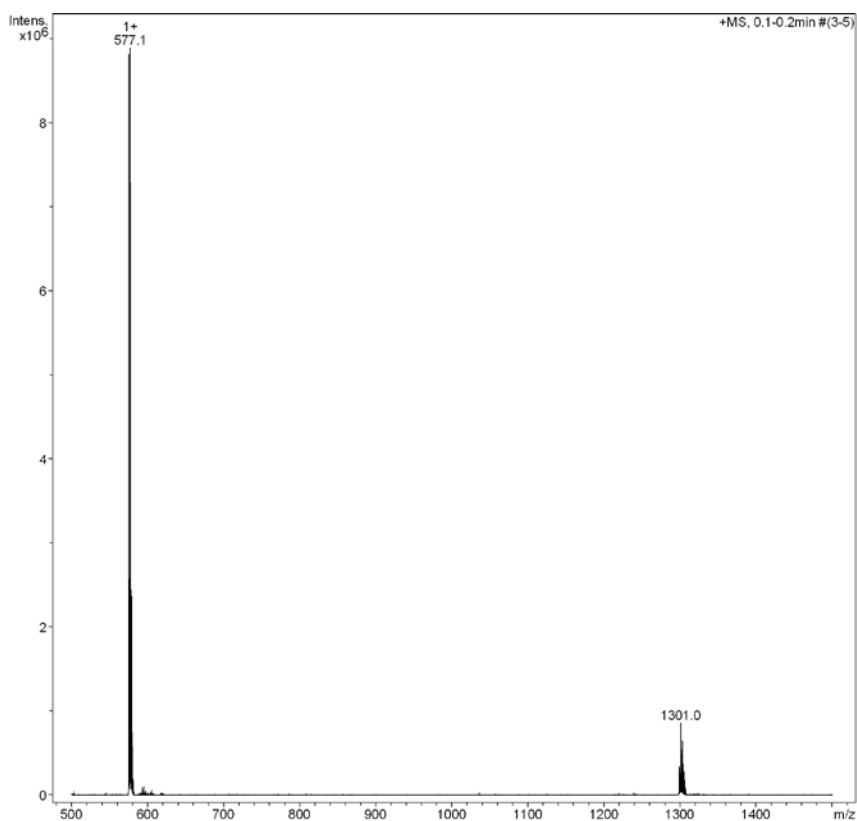


Figure S9. ESI-MS of a CH₃CN solution of isolated complex **1t**.

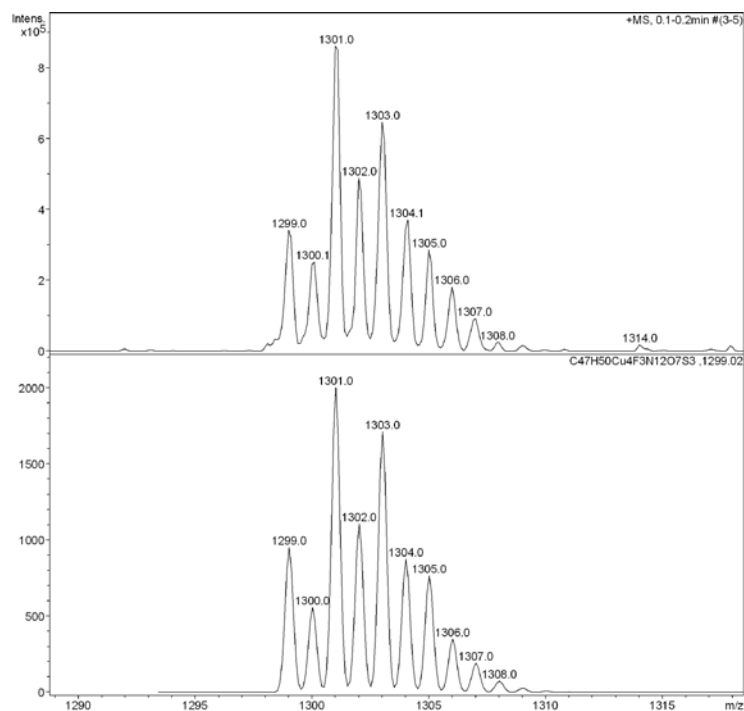
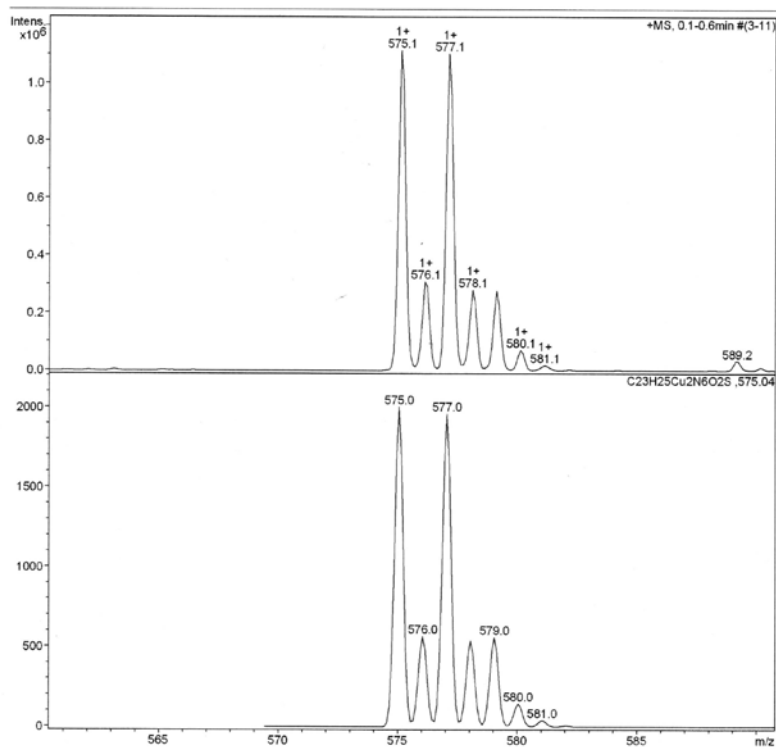
A**B**

Figure S10. Experimental (top) and theoretical (bottom) isotopic pattern from (A) $[(\text{Cu}_4(\text{L}^{\text{MeH}})_2(\mu\text{-OH})_2(\text{OTf}))^+]$ and (B) $[\text{Cu}_2(\text{L}^{\text{MeH}})(\mu\text{-OH})^+]$.

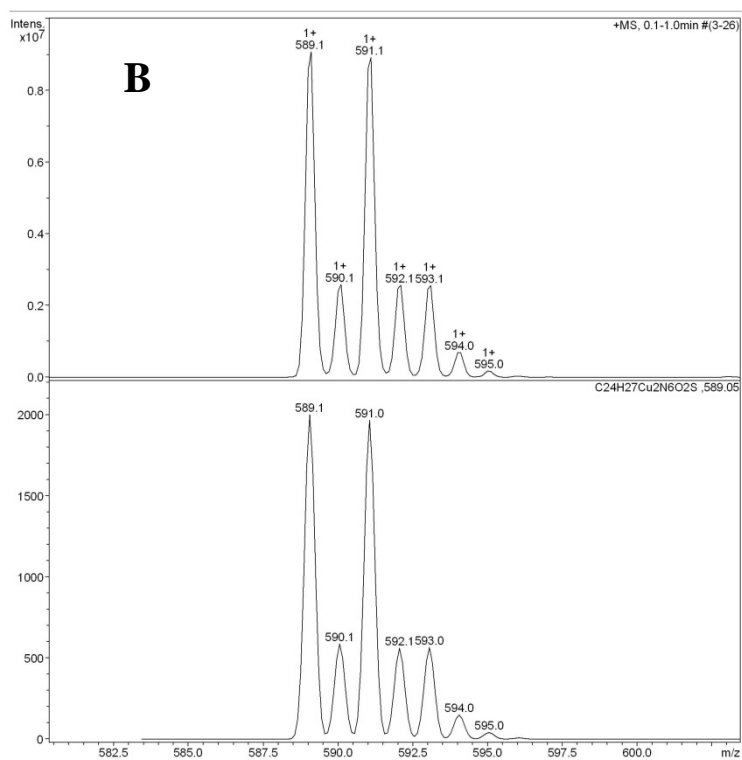
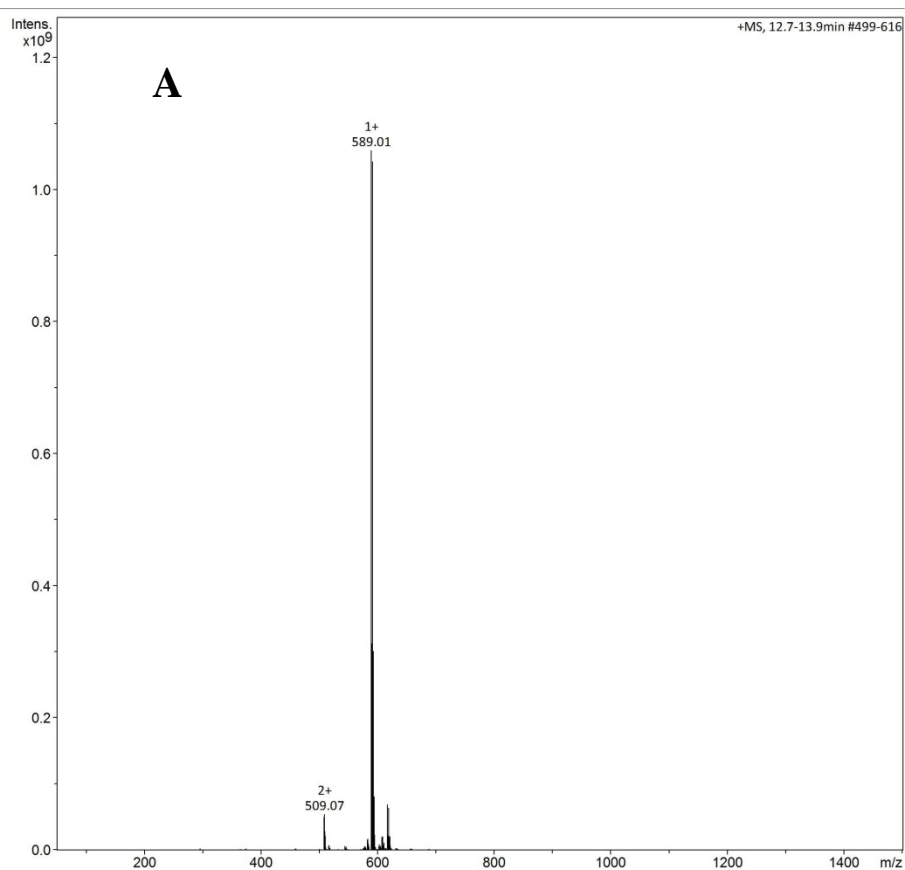


Figure S11. (A) ESI-MS of a CH₃CN solution of isolated complex **2d**; (B) Experimental (top) and theoretical (bottom) isotopic pattern for [Cu₂(L^{Me2})(μ-OH)]⁺

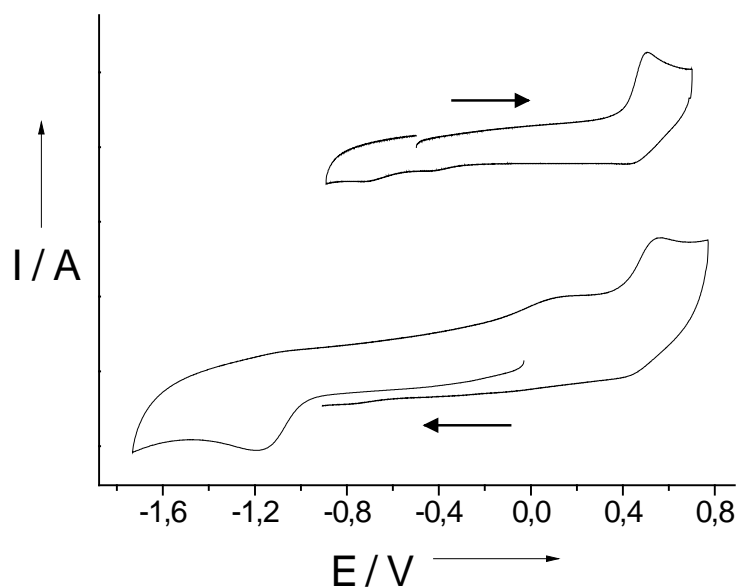


Figure S12. CVs of a 1 mM solution of **1t** in CH₃CN. The arrows indicate the starting potential and direction of each scan. Conditions: Scan rate: 200 mV·s⁻¹, 0.1 M TBA·PF₆ (supporting electrolyte), glassy carbon working electrode. T = 298 K. The potentials are referenced versus the Fc⁺/Fc redox couple.

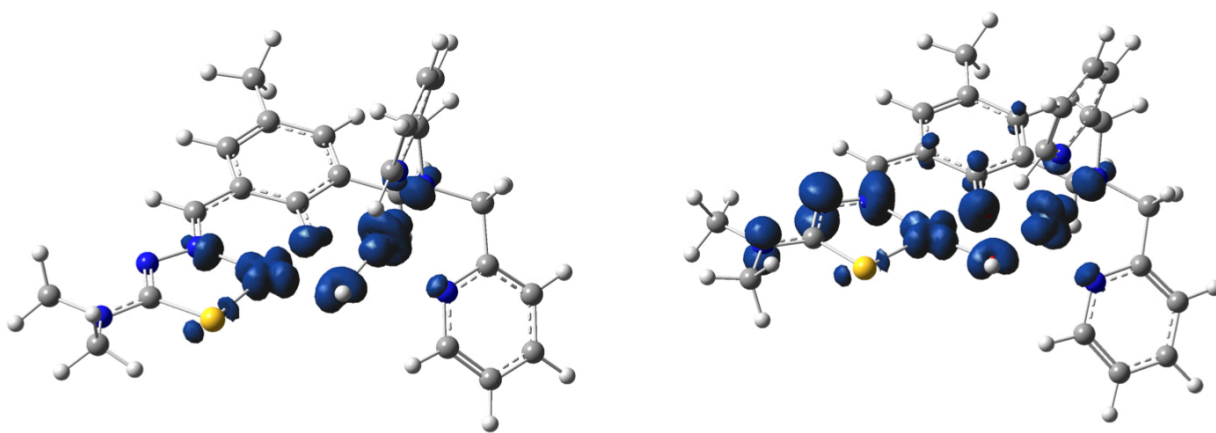


Figure S13. Spin density plot (isosurface equals to 0.01 ua) for the high spin state of **2d** (left) and for its mono-oxidized species (right).

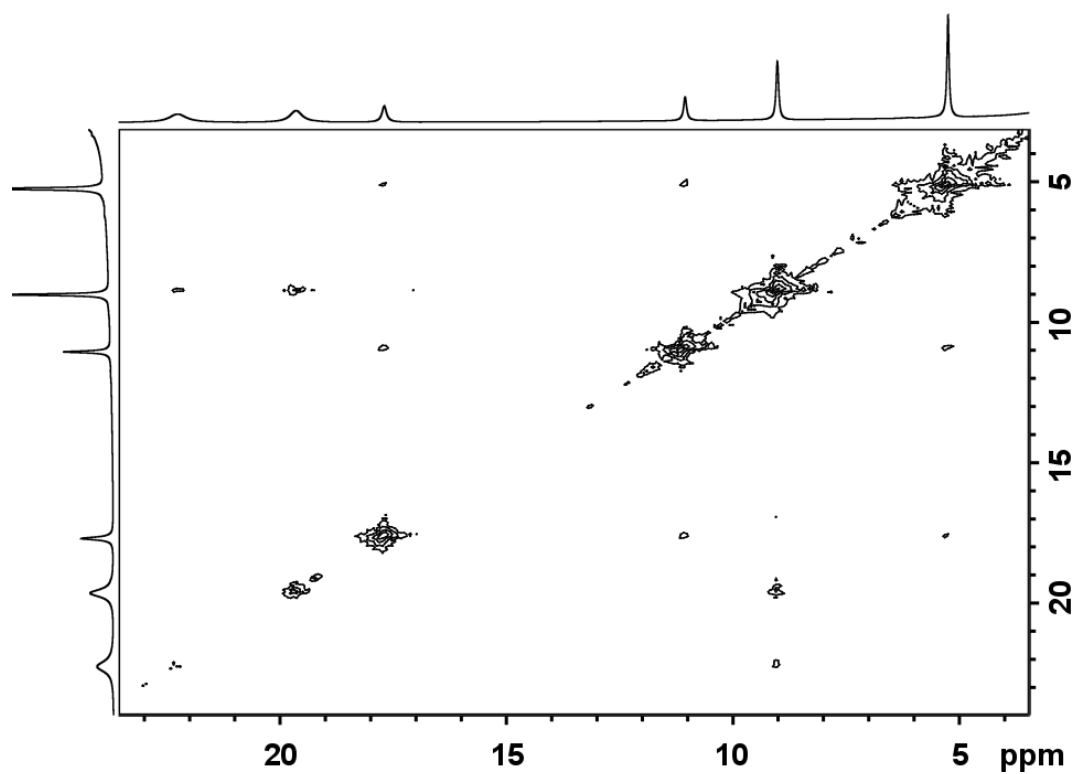


Figure S14. COSY spectrum of complex **1t** taken in CD₃CN at 298 K

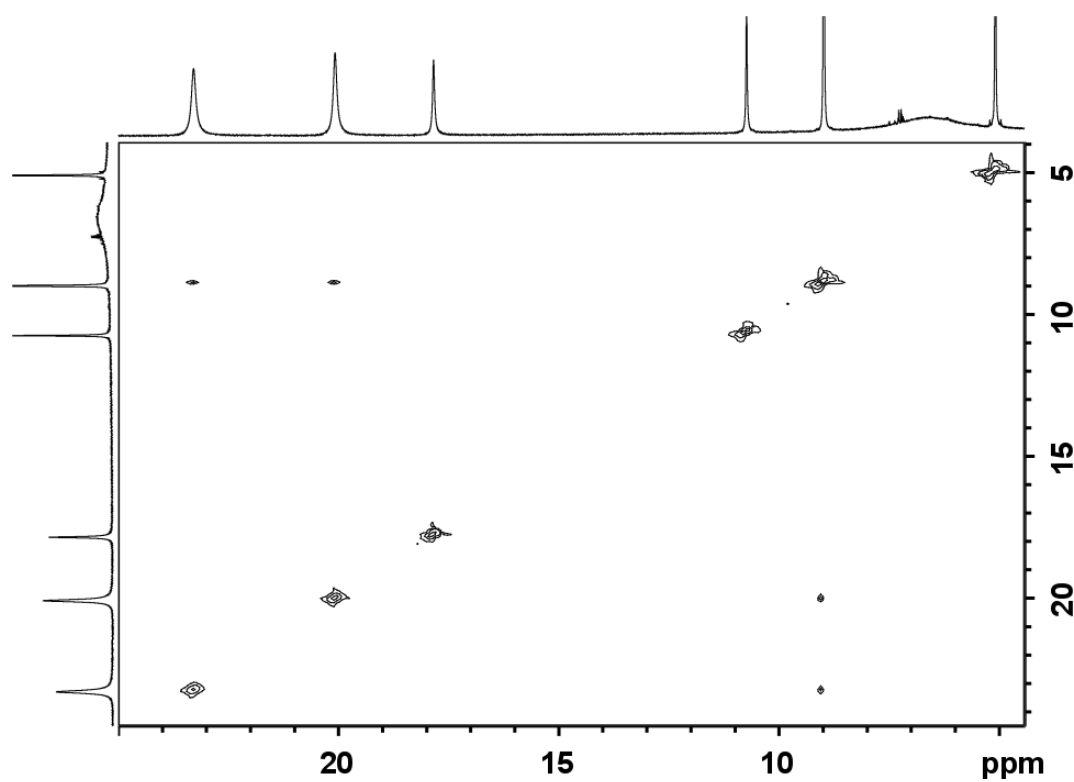


Figure S15. COSY spectrum of complex **2d** taken in CD₃CN at 298 K

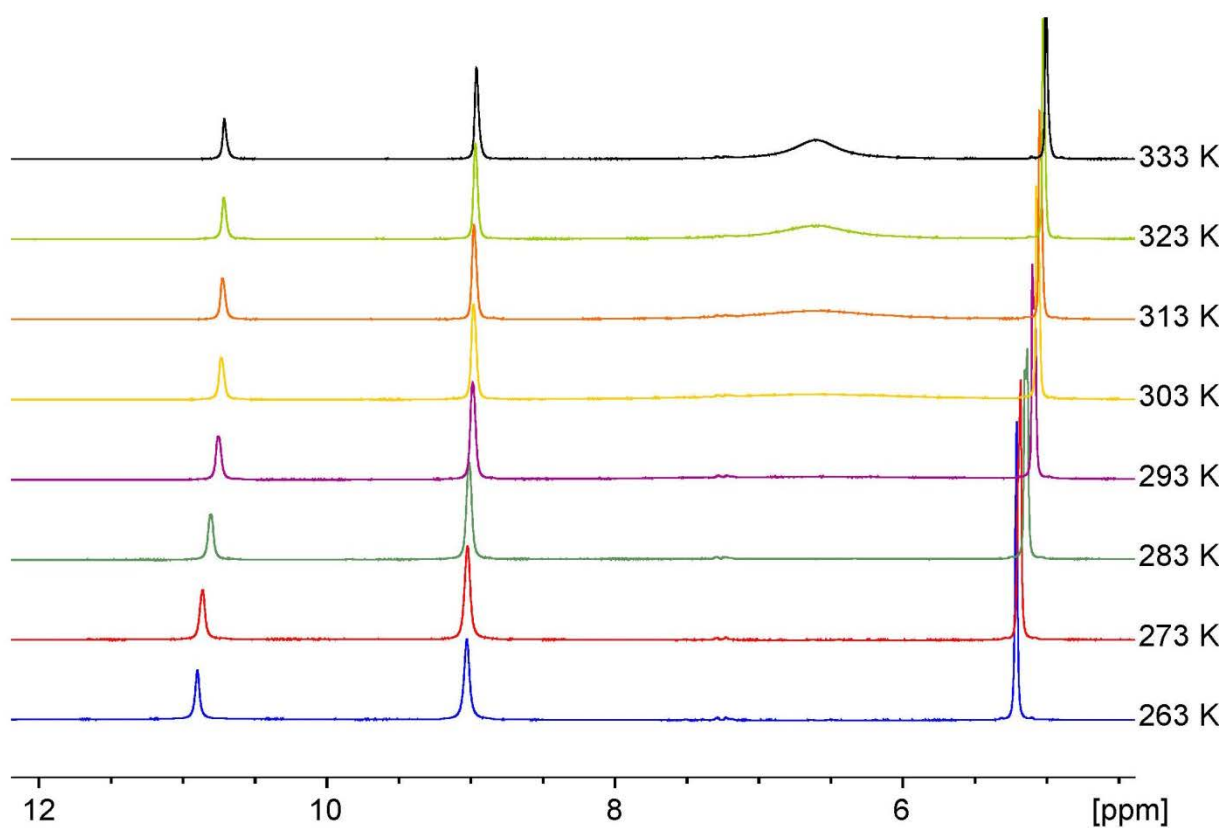


Figure S16. Variable temperature ¹H NMR spectra for complex **2d** in solution (CD₃CN).

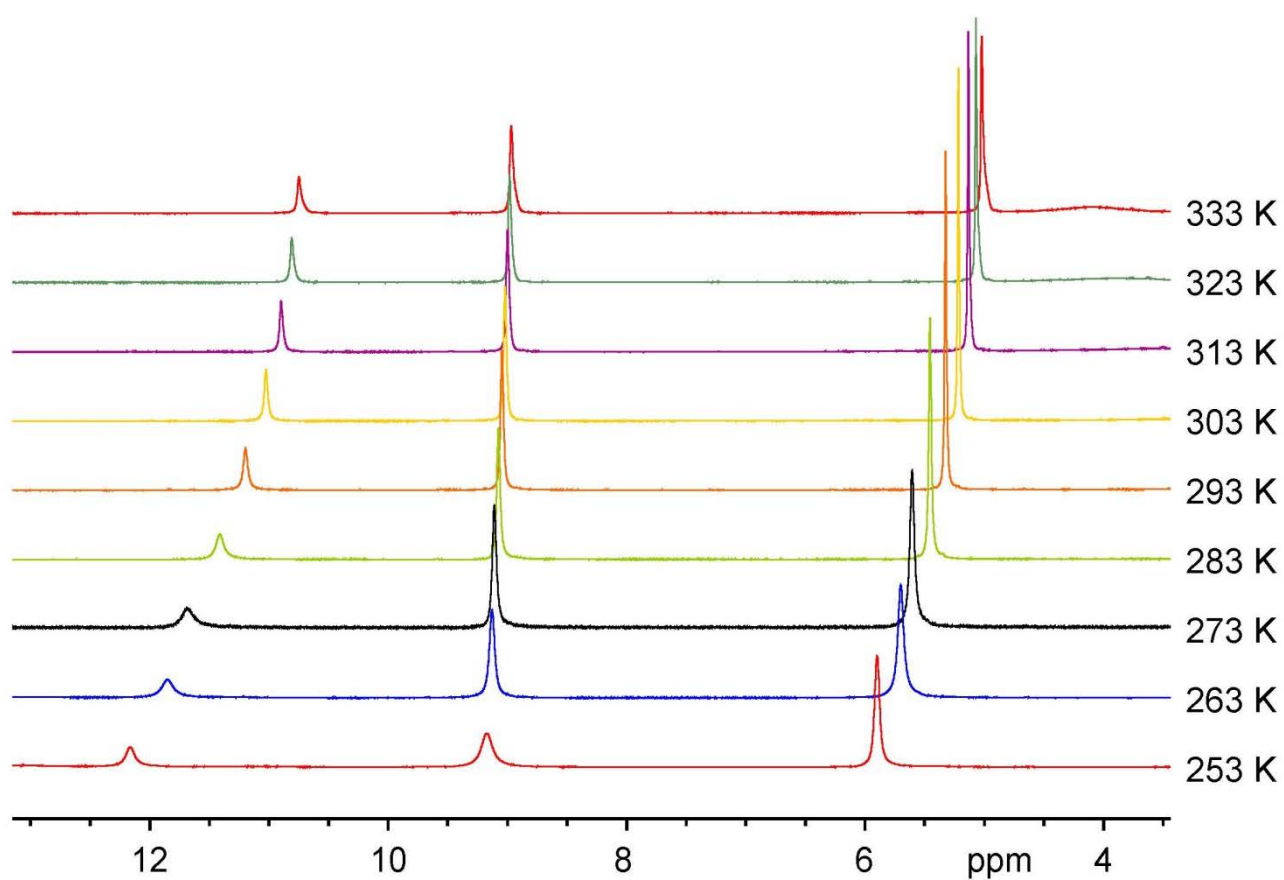


Figure S17. Variable temperature ¹H NMR spectra for complex **1t** in solution (CD₃CN).

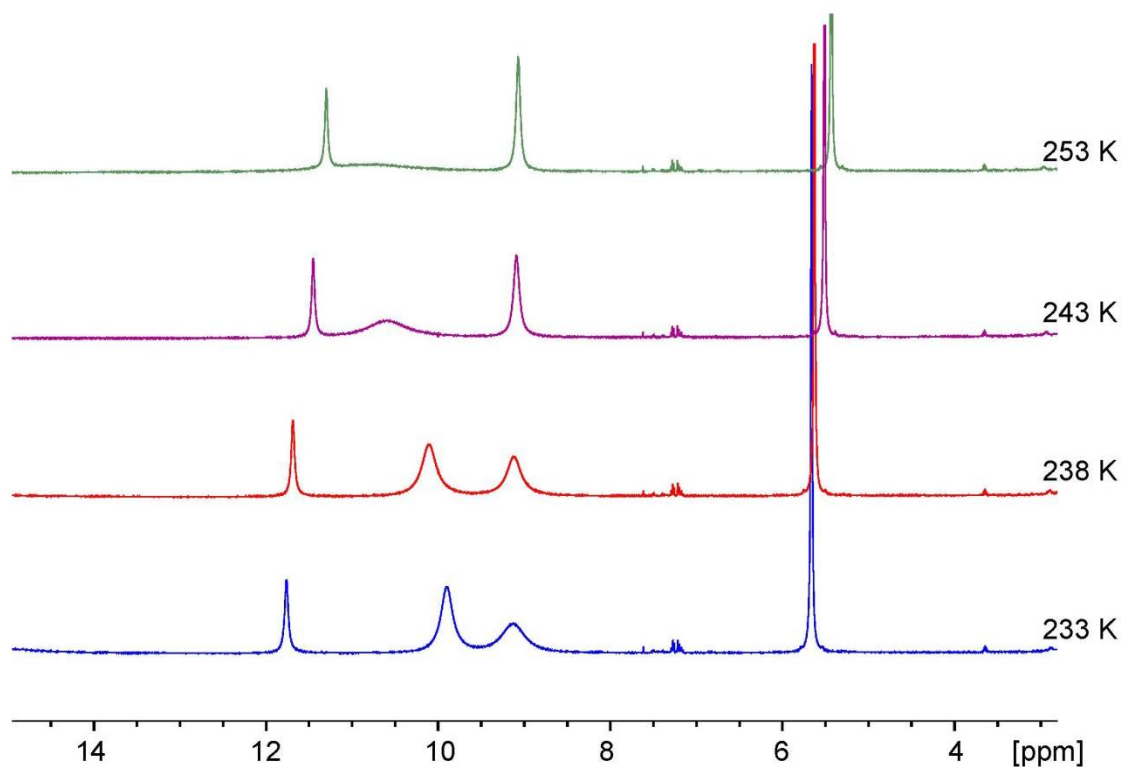


Figure S18. Portion of ¹H NMR spectra of complex **2d** in solution at different temperature (253K to 233K). The appearance of the peak at 10 ppm is probably due to molecular dynamics processes slowed below 253K. This additional resonance is expected to be closer to the Cu(II) ions causing a severe line broadening and precluding assignment of this peak.

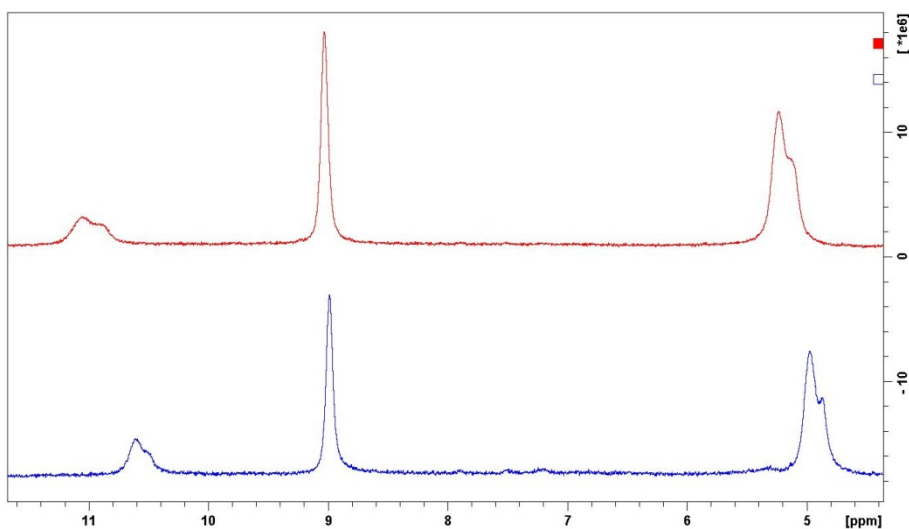


Figure S19. Portion of ^1H HRMAS spectra of complex **1t** (top) and complex **2d** (low) in presence of LiChrospher 100 RP-18 (5 μm) chromatographic stationary phase.

Table S1. Main geometric parameters of **1t** and **2d** after geometry optimisations computed at IEFPCM/PBE0 level. Data for crystal structures are given in parenthesis, distances are in \AA and angles in degree. Notations correspond to the figures 2 and 3.

	1t	2d
Cu1.....Cu2	2.979(2.9551(11))	2.979(2.9842(11))
Cu2.....Cu1'	3.491(3.491(1))	-
Cu1.....S1	2.287(2.2413(8))	2.252(2.2107(11))
Cu1.....O1	1.989(1.9589(17))	1.956(1.936(2))
Cu1.....O2	1.996(1.9616(18))	1.959(1.930(2))
Cu1.....O2'	2.331(2.4089(18))	-
Cu1.....N2	1.970(1.939(2))	1.960(1.926(2))
Cu2.....O2	1.958(1.9342(17))	1.935(1.905(2))
Cu2.....O1	2.028(2.0072(18))	2.098(2.058(2))
Cu2.....N1	2.054(2.018(2))	2.044(2.019(2))
Cu2.....N4	2.024(1.979(2))	2.060(2.013(3))
Cu2.....N5	2.267(2.253(2))	2.069(2.041(3))
S1.....C10	1.758(1.747(3))	1.760(1.749(3))
C10.....N3	1.306(1.307(3))	1.314(1.325(4))
O2-Cu1-S1	99.02(97.65(5))	99.96(99.89(7))
O2'-Cu1-S1	96.42(93.97(5))	-
O1-Cu1-O2	80.78(81.11(7))	81.54(79.45(9))
O1-Cu2-O2	80.72(80.57(7))	78.58(77.03(9))
N2-Cu1-S1	85.55(86.53(6))	86.26(87.93(8))
N2-Cu1-O2	164.80(164.14(8))	172.29(170.20(9))
N2-Cu1-O1	92.64(92.90(8))	92.64(92.64(10))
Cu1-O1-Cu2	95.75(96.33(8))	94.52(96.65(9))
Cu1-O2-Cu2	97.77(98.67(8))	99.80(102.19(9))